Published by The College of Science & Information Technology (COSIT), TASFUED, Vol. 20, No. 1, pp. 189-203.

COSIT, TASFUED
Journal of Science and Information Technology (JOSIT)

Adsorption characteristics of Fe-doped graphitic carbon nitride/PEDOT polymer hybrid material as sensors for dissolved gases in the transformer oil: A DFT study

[1]Ntui, T. N.; [2]Kalu, D. M.; [3]Badeji, A. A.; [4]Louis, H.

[1]Department of Industrial Chemistry. University of Cross River State, Calabar, Nigeria.
[2]Department of Pure and Industrial Chemistry, University of Calabar, Calabar, Nigeria.
[3]Department of Chemical Sciences, Tai Solarin Federal University of Education, Ijagun, Ogun State, Nigeria.
[4]Department of Pure and Industrial Chemistry, University of Calabar, Calabar, Nigeria.

Corresponding Author: ogunlanaaa@tasued.edu.ng; ORCID: 0000-0002-9952-4618

Abstract

This study evaluates the adsorption potency of a hybrid nanomaterial composed of Fe-doped graphitic carbon nitride-poly (3,4 -ethylenedioxythiophene) (Fe@C_3N_4-PEDOT) towards acetylene (C_2H_2), methane (CH_4), and hydrogen (H_2) gases. Density functional theory (DFT) was employed to optimize the structures and to evaluate or examine the electronic properties, adsorption, and interaction behaviour. Adsorption energies (Eads) for C_2H_2 (-0.871 eV), H_2 (-0.381 eV), and CH_4 (-0.381 eV) specify exothermic and spontaneous interactions. C_2H_2 (-0.871 eV) shows moderate chemisorption, while CH_4 and H_2 (-0.381 eV each) show weak chemisorption, within the reusable sensor range. The C_2H_2 showed greater interaction, reducing the energy gap to 2.256 eV, thereby improving conductivity and reactivity. Density of States (DOS) was equally confirmed, as it reveals a significant orbital overlap between the gas and the studied material. Natural Bond Orbital (NBO) analysis also showed a good donor-acceptor interaction with high stabilization energy, which affirms chemisorption. The hybrid nanomaterial's interaction with these gases, especially acetylene, suggests its high suitability for selective detection and adsorption of hazardous gases in oil and oil-polluted environments. In all, Fe@C_3N_4-PEDOT shows promising potential as a sensor material with high sensitivity and environmental importance.

Keywords: Graphitic carbon; PEDOT; Adsorption; Transformer oil; DFT

INTRODUCTION

Oil-dissolved gases have become a major concern, particularly in the crude oil processing and transformer oil system, which contributes to a larger proportion in the transmission of power, due to their linkage with thermal degradation and electrical faults [1,2]. This transformer oil undergoes a chemical decomposition on exposure to high temperatures, electrical discharge, or arcing, which leads to the generation of gases such as acetylene (C_2H_2), methane (CH_4), and hydrogen (H_2), serving as early indicators of faults in power transformers [1,3,4]. According to previous studies, it is observed that the formation of CH_4 indicates low-energy thermal faults ranging from 150-300 °C, while C_2H_2 is linked to the high-energy discharge [3]. The H_2 is the lightest and a product of partial discharge and one of the causes of insulation breakdown [3,5,6]. Conversely, for crude oil, the accumulation of these gases suggests aging or product degradation, affecting both quality and safety [7,8]. The presence of these gases poses risks of fire outbreak/explosion and long-term instability of the system. Therefore, there is a need for accurate detection and effective

Cite as:

Ntui T. N., Kalu D. M., Badeji A. A., Louis, H. (2026). Adsorption characteristics of Fe-doped graphitic carbon nitride/PEDOT polymer hybrid material as sensors for dissolved gases in the transformer oil: A DFT study. *Journal of Science and Information Technology (JOSIT)*, Vol. 20, No. 1, pp. 189-203.

sensing of these gases, as it enhances the maintenance, safety, and performance of our system. Although conventional approaches such as gas chromatography and infrared spectroscopy have been widely used in the analysis of oil-dissolved gases often cost-ineffective, labour-intensive, and require pre-treatment, lacking instant monitoring ability [9, 10]. These limitations have shifted the attention of researchers towards materials that can adsorb or sense gases directly in oil, avoiding the preprocessing steps by conventional methods. In this light, nanomaterials are emerging efficiently due to their porosity and tuneable electronic properties [11, 12, 13].

Computational studies using density functional theory (DFT) have shown the great potential of nanoengineered materials for oil-dissolved gases sensing. For example, CuO-decorated boron nitride nanotubes (BNNTS) showed good interaction with acetylene (C_2H_2) but weak response to methane (CH_4), and hydrogen (H_2), which limits their application for different gas sensing [14]. Also, a Pd- and Pt-doped ZnO monolayer system showed good sensitivity towards C_2H_2 and H_2, gases but failed to address the adsorption recovery [15]. Likewise, Ni-decorated PtS_2 was studied for CO and C_2H_2 sensing, which offered high sensitivity. However, the desorption was too slow for continuous application [16]. Despite these advancements, there remains a need to engineer materials for high sensitivity, selectivity, and reversibility in the gases under study.

To address these limitations, we investigate a hybrid nanomaterial composed of iron-based graphitic carbon nitride ($Fe@C_3N_4$) combined with a conductive polymer, PEDOT. The C_3N_4 gives chemical stability, nitrogen-rich and high electron-donating ability, making it good for transition metals like Fe doping, which is aimed at introducing active sites for gas interaction, and PEDOT contributes conductivity, improves electron mobility, and stabilizes the nanostructure [17,18]. $Fe@C_3N_4$–PEDOT material serves as a promising material for sensing of CH_4, C_2H_2, and H_2. Using DFT at the B3LYP/LanL2DZ level, we assess certain parameters such as adsorption energy, electronic properties (DOS, HOMO–LUMO gap), and natural bond orbital interactions to evaluate the potential of the material with improved sensitivity, selectivity, and reversibility.

COMPUTATIONAL DETAILS

For this study, all calculations were done using the density functional theory (DFT) method as implemented in the Gaussian 16 software. LanL2DZ basis set was used for this study due to its suitability for transition metal systems, especially for Fe, and its effective core potentials [19]. The B3LYP functional was used throughout the study because of its accuracy in molecular systems [20]. Vibrational frequency calculations were carried out to confirm that the optimized structures were true minima, with no imaginary frequency. In understanding the gas-surface interactions, HOMO-LUMO, Density of states (DOS), natural bond orbitals (NBO), Adsorption energy, non-covalent interactions (NCI), and quantum theory of atoms in molecules (QTAIM) were carried out and analysed using Multiwfn and visualized using VMD, Chemcraft, and GaussView [21].

Table 1. Structural results for the four interacting complexes based on bond length evaluation.

Systems	Bond label	Bond distance (Å)	
		Before	After
C_2H_2	C_1 -H_3	1.068	-
CH_4	C_1 - H_3	1.095	-
H_2	H_1-H_2	0.743	-
C_2H_2-Fe@C3N4-PEDOT	C_{113}-H_{115}	1.068	1.074
	C_{113}-Fe_{111}	-	2.018
	C_{112}-Fe_{111}	-	2.023
CH_4-Fe@C3N4-PEDOT	C_{112}-H_{114}	1.095	1.097
	C_{112}-Fe_{111}	-	2.847
H_2-Fe@C3N4-PEDOT	H_{112}-H_{113}	0.743	0.767
	H_{112}-Fe_{111}	-	1.943
	H_{113}-Fe_{111}	-	1.962

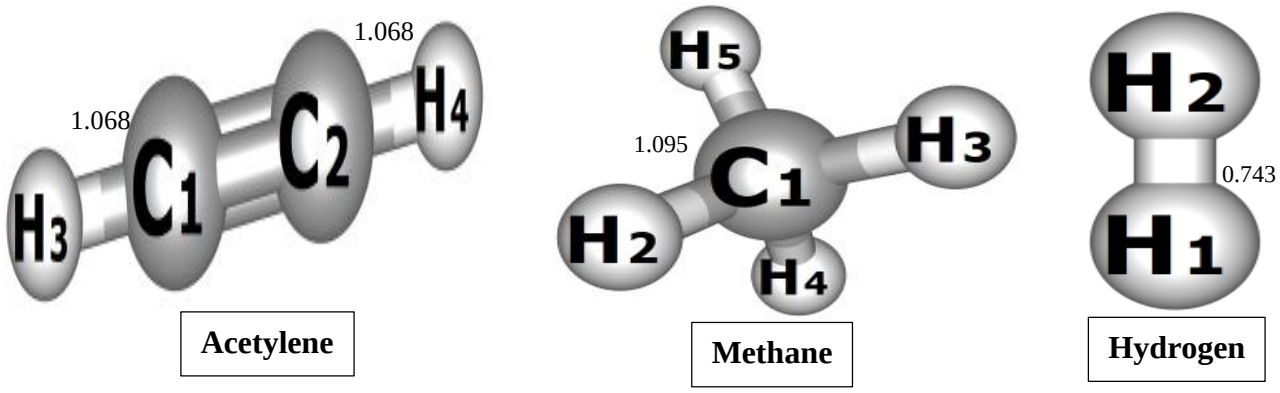

Figure 1 (a). Geometric structures of the adsorbates: C_2H_2, CH_4, H_2.

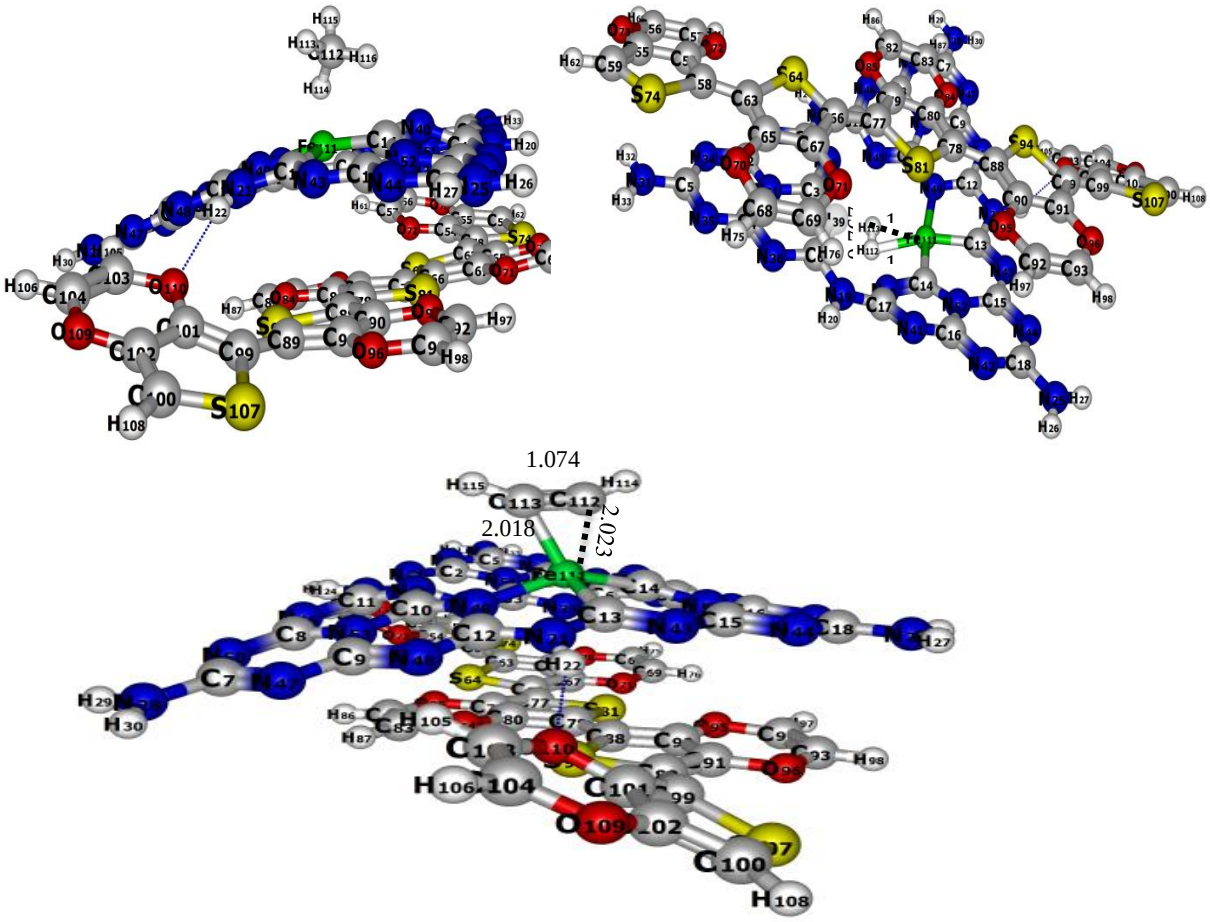

Figure 1 (b). Geometric structures of Fe@C_3N_4-PEDOT interactions with the adsorbates.

RESULTS AND DISCUSSION

Geometric Optimization

Optimization of geometry was carried out in this study for CH_4, C_2H_2, and H_2 gases before and after interaction on the Fe@C_3N_4–PEDOT surface using the B3LYP/LanL2DZ DFT method. The optimized bond lengths of the isolated gases are: C–H in C_2H_2 (1.068 Å), C–H in CH_4 (1.095 Å), and H–H in H_2 (0.743 Å). However, on interaction with the surface material, there was a slight elongation of the internal bond in —C–H in C_2H_2 to 1.074 Å, C–H in CH_4 to 1.097 Å, and H–H in H_2 to 0.767 Å, proposing a level of structural distortion. Also, new bond formation was observed between the Fe active site and atoms from each system. As shown in Table 1 below, C_2H_2 showed Fe-C bond distances of 2.018 Å and 2.023 Å, suggesting a stronger interaction in comparison to CH_4, which had a Fe-C distance of 2.847 Å. This suggests a shorter bond length is indicative of a stronger interaction [22]. The H_2 molecule on interaction with Fe had a bond length of 1.943 Å and 1.962 Å with a slightly stretched H-H bond from 0.743 – 0.767 Å. These structural adjustments suggest an occurrence of adsorption of the gases on interaction with the Fe@C_3N_4–PEDOT surface, with the most significant geometric changes observed in C_2H_2 and H_2 complexes.

Electronic properties

1. **Density of States DOS**

The density of states (DOS) was employed to unravel the change in electronic properties and to envision the movement of electrons from the valence band to the conduction band of the investigated interactions, and the order of arrangement of quantum states at various energy levels [23]. The study evaluates the contribution of each atomic fragment of the interacting systems under investigation in consideration with other related DOS parameters such as Total Density of States (TDOS), Orbital Projection density of states (OPDOS), and lastly Partial Density of States (PDOS), which represent the

orbital of the atomic fragments. The studied interactions consist of a carbon atom (C), a Nitrogen atom (N), a hydrogen atom (H), a sulphur atom (S), and an Oxygen atom (O) with the substituent metal atom Iron (Fe). As presented in Figure 2, the system exhibits slightly different Fermi energy levels: -6.48 eV for C_2H_2-Fe@C_3N_4-PEDOT, -6.57 eV for CH_4-Fe@C_3N_4-PEDOT, -6.63 eV for H_2-Fe@C_3N_4-PEDOT, and the bare system -6.54 eV Fe@C_3N_4-PEDOT. This level depicts the highest occupied electron state at absolute zero temperature and serves as a reference point for electron transfer processes. The plots revealed that C atoms contribute more significantly from the valence band region and across the energy range, N atoms contribute particularly in the -15 to -10 eV range, which peaks close to the Fermi energy levels, and Fe atoms demonstrate sharp peaks specifically from the characteristic d-orbital contribution. Meanwhile, on the PEDOT S and O atoms contributed mainly in the minimal energy region, as H atoms are observed with a minor contribution in the entire plots. In the systems, C3N4 enhances the semiconductor framework in the systems, Fe brings about catalytically active sites due to the accessible d-states [24], while PEDOT enhances conductivity and charge transfer. The collective contribution of the fragment systems via the hybridization result of the DOS may greatly improve sensing and adsorption due to enhanced charge separation and transfer. Hence, it is evident that the Fe atom plays a crucial role in the systems, because of the d-states close to the Fermi level, suggesting the systems with enhanced reactivity and potential for strong gas-surface interactions. Conversely, system C_2H_2-Fe@C_3N_4-PEDOT portrays strong interaction due to the difference in the C atom contributions, system CH_4-Fe@C_3N_4-PEDOT was suggested with moderate binding due to the modified electronic structure, and H_2-Fe@C_3N_4-PEDOT shows a distinct change in the DOS pattern.

2. HOMO-LUMO Analysis

Frontier molecular orbital (FMO) enhances the understanding of the electronic properties of the studied systems by evaluating their sensitivity, reactivity, conductivity, and stability [25]. It also offers a thorough insight into intermolecular interactions. To address the highlighted points of interest, we focus on various parameters such as the Highest Occupied Molecular Orbital (HOMO), Lowest Unoccupied Molecular Orbital (LUMO), Energy Gap (Egap), and the global quantum chemical descriptors. The HOMO and LUMO iso-surface plots as presented in Figure 3 revealed that electrons are localized close to the Fe site in all the systems, and electrons are delocalized mostly towards the adsorbates and PEDOT. Although there is a strong orbital overlapping (Hybridization) in system C_2H_2-Fe@C_3N_4-PEDOT compared to system H_2-Fe@C_3N_4-PEDOT, leading to improved sensing potential. The studied systems exhibit a semiconductor energy gap of less than three electron volt (<3 eV). Egap is informative on the structural stability, polarizability, and chemical reactivity of the studied systems. Hence, a large Egap indicates a chemically hard system with high stability, while a lower Egap indicates that the system is chemically soft and reactive [26]. According to the result in Table 2, systems C_2H_2-Fe@C_3N_4-PEDOT portray higher reactivity attributing to lower value of 2.256 eV band gap compared to system CH_4-Fe@C_3N_4-PEDOT with moderate reactivity due to slight increase in the band gap value of 2.273 eV, while system H_2-Fe@C_3N_4-PEDOT (2.255 eV) and C_2H_2-Fe@C_3N_4-PEDOT (2.256 eV) exhibit virtually identical Egap values (difference of 0.001 eV is within computational precision), while CH_4-Fe@C_3N_4-PEDOT (2.273 eV) is least reactive. The band gap revealed that systems C_2H_2-Fe@C_3N_4-PEDOT and H_2-Fe@C_3N_4-PEDOT exhibit more reactivity due to increased softness value and electrophilicity compared to system CH_4-Fe@C_3N_4-PEDOT.

The chemical descriptors greatly influence the chemical properties of the investigated systems. Hence, the ionization potential (IP) represents the strength of electron donation, while electron affinity (EA) implies the tendency of electron acceptance [27]. The systems demonstrate approximately IP values of 5.1 eV and 2.9 eV for electron affinity, signifying a balance of donor and acceptor characteristics. Chemical hardness (η) and chemical softness (σ) parameters revealed that the systems portray less stability and resistance to deformation, with approximately η values of 1.1 eV and high reactivity attributed to the approximately softness values of 0.89 eV. Chemical potential (μ) measures the tendency to gain an electron, while electronegativity measures the electron attraction potency of the system [28]. As per Koopman's theorem, electronegativity $\chi = (IP+EA)/2$ measures the tendency to attract electrons, while chemical potential $\mu = -\chi = -(IP+EA)/2$ is its negative, representing the tendency to donate electrons. The values in Table 2 confirm this

relationship. Lastly, the systems possess high electrophilic properties, especially in system H2-Fe@C_3N_4-PEDOT, with an approximate electrophilicity index (ω) value of 7.3 eV, indicating the ability to accept electrons (electrophilic). Whereas the bare surface exhibits increased values in all the parameters, suggesting stability of the surface before interaction. The descriptors were calculated mathematically employing Koopman's theory as shown in equations (1) – (7). Interestingly, the analysis revealed that materials are sensitive in the following order: C_2H_2-Fe@C_3N_4-PEDOT, H_2-Fe@C_3N_4-PEDOT, and CH_4-Fe@C_3N_4-PEDOT, making it ideal for the study interest.

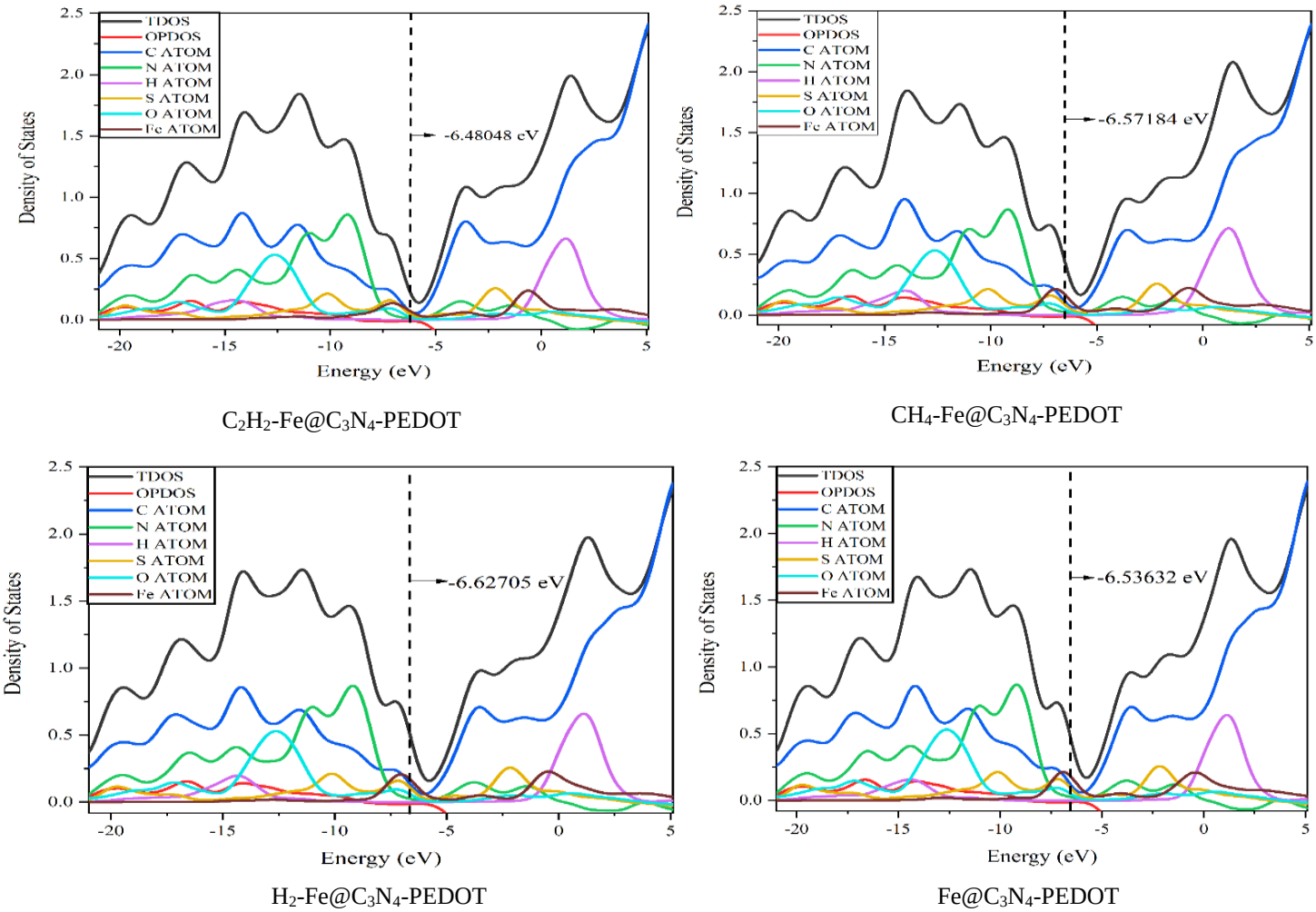

C_2H_2-Fe@C_3N_4-PEDOT

CH_4-Fe@C_3N_4-PEDOT

H_2-Fe@C_3N_4-PEDOT

Fe@C_3N_4-PEDOT

Figure 2. Density of States plots for the studied interaction and the bare surface.

$$\text{Ionization potential (IP)} = -E_{HOMO} \quad (1)$$
$$\text{Electron Affinity (EA)} = -E_{LUMO} \quad (2)$$
$$\text{Chemical Hardness (η)} = (IP - EA)/2 \quad (3)$$
$$\text{Chemical softness (σ)} = 1/\eta \quad (4)$$
$$\text{Chemical potential (μ)} = -(IP + EA)/2 \quad (5)$$
$$\text{Electronegativity } (\chi) = (IP + EA)/2 \quad (6)$$
$$\text{Electrophilicity (ω)} = \mu^2/2\eta \quad (7)$$

Table 2. HOMO, LUMO, and quantum descriptors results for studied interactions and the bare surface.

Systems	E_{HOMO} eV	E_{LUMO} eV	E_{gap} eV	IP eV	EA eV	η eV	σ eV	μ eV	χ eV	ω eV
C2H2-Fe@C3N4-PEDOT	-5.166	-2.910	2.256	5.166	2.910	1.128	0.887	-4.038	4.038	7.227
CH4-Fe@C3N4-PEDOT	-5.192	-2.919	2.273	5.192	2.919	1.137	0.880	-4.056	4.056	7.234
H2-Fe@C3N4-PEDOT	-5.191	-2.936	2.255	5.191	2.936	1.128	0.887	-4.064	4.064	7.321
Fe@C3N4-PEDOT	-5.209	-2.937	2.272	5.209	2.937	1.136	0.880	-4.073	4.073	7.301

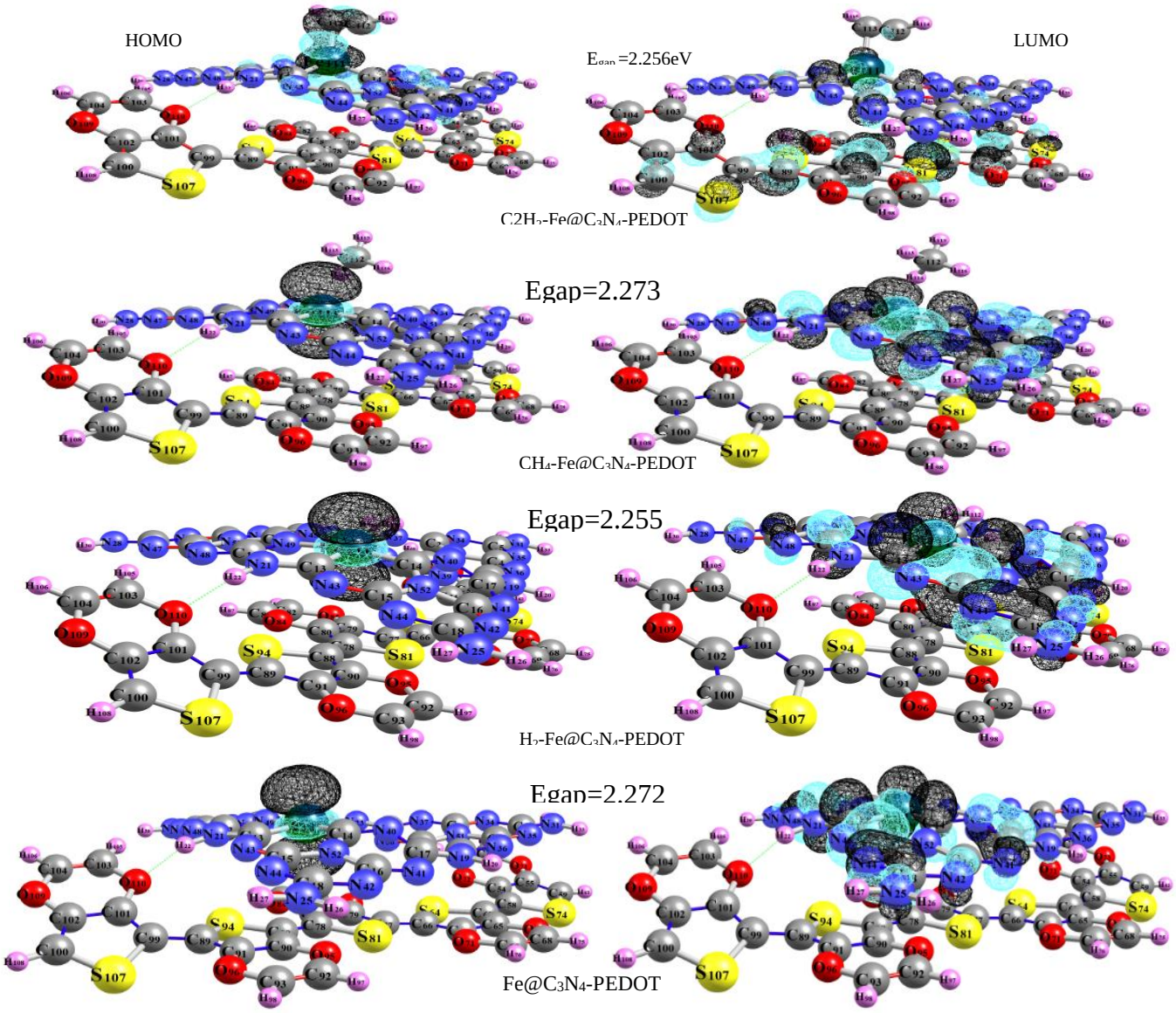

Figure 3. HOMO LUMO iso-surface plots for the investigated interactions and the bare surface.

Table 3. NBO result for the studied interactions and the bare surface.

Compound	Donor (i)	Acceptor (j)	$E^{(2)}$ Kcal/mol	E(j)-E(i) a.u	F (i, j) a.u
C2H2-Fe@C3N4-PEDOT	LP^{*} Fe_{111}	σ^{*} C_{14} -Fe_{111}	201.46	0.04	0.268
	LP^{*} Fe_{111}	σ^{*} C_{13} -Fe $_{111}$	203.24	0.03	0.222
	σ Fe $_{111}$ - C $_{113}$	LP^{*} C_{112}	288.20	0.21	0.337
CH4-Fe@C3N4-PEDOT	π^{*} C_{10} - N_{49}	π^{*} C $_{11}$ - N_{45}	111.93	0.02	0.07
	σ^{*} C_{14} -Fe $_{111}$	σ^{*} C_{13} -Fe $_{111}$	144.87	0.03	0.196
	π^{*} C_{13} - N_{21}	π^{*} C $_{15}$ - N_{43}	146.03	0.01	0.078
H2-Fe@C3N4-PEDOT	π^{*} C_{10} - N_{49}	π^{*} C_{11} – N_{45}	109.80	0.02	0.075
	σ^{*} C_{14} -Fe $_{111}$	σ^{*} C $_{13}$ -Fe $_{111}$	130.45	0.03	0.171
	π^{*} C_{12} - N_{21}	π^{*} C $_{9}$ - N_{48}	165.16	0.01	0.075
Fe@C3N4-PEDOT	π C_{14} - N_{40}	LP^{*} C_{17}	110.03	0.08	0.128
	π^{*} C $_{18}$ - N $_{42}$	π^{*} C_{15} - N_{44}	157.45	0.01	0.074
	LP Fe 111	π^{*} C_{13} - N_{43}	271.03	0.05	0.149

Table 4. Calculated adsorption energies of the studied systems.

Systems	Energy of the complex a.u	Energy of the surface a.u	Energy of the Adsorbates a.u	Adsorption energy a.u	Adsorption energy eV
C2H2-Fe@C3N4-PEDOT	-4267.994	-4190.644	-77.318	-0.032	-0.871
CH4-Fe@C3N4-PEDOT	-4231.173	-4190.644	-40.515	-0.014	-0.381
H2-Fe@C3N4-PEDOT	-4191.832	-4190.644	-1.174	-0.014	-0.381

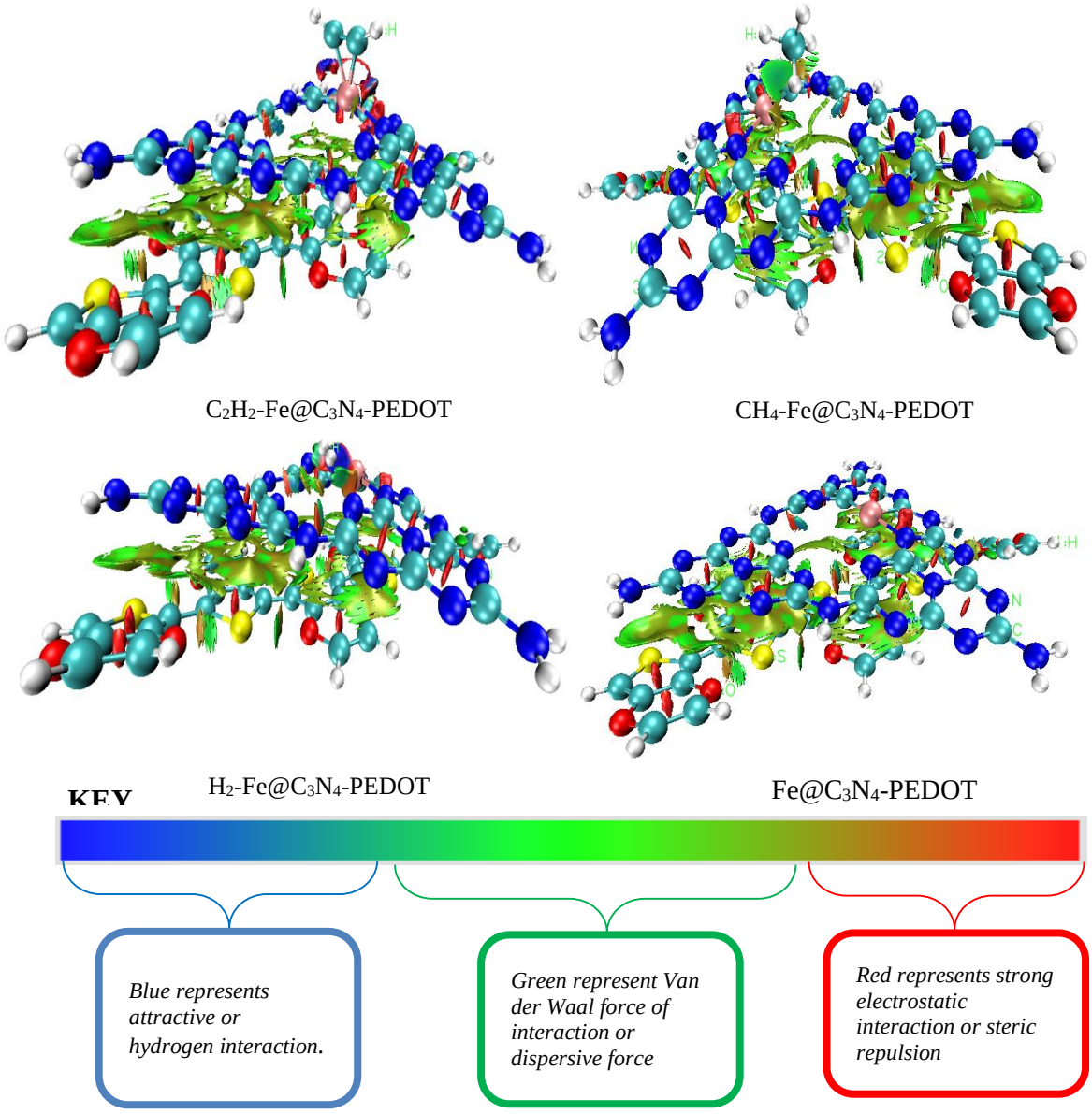

Figure 4: NCI iso-surface plots for the investigated interactions and the bare surface

Natural Bond Orbital (NBO)

Conjugation and hyper-conjugation interaction with the intermolecular charge transfer and how electron delocalization occurs between the donor and acceptor of the gas to be adsorbed and the studied surface was unveiled through Natural Bond Orbital (NBO). This approach comprehensively breaks the complex Schrödinger equation into a more understandable form through chemical bond concepts [29]. The strength of the interaction between the two orbitals (donor and acceptor) is quantified by the stabilization energy (E2). Higher (E2) implies effective adsorption of the sensing material resulting from a strong interaction between the donor and acceptor orbitals [30]. The analysis focused on the following bond types: sigma (σ), anti-sigma (σ*) bonds, pi-bonds (π), anti-pi-bonds (π*), and lone pairs (LP). E(j) – E(i) quantifies the difference between the acceptor orbital representing the energy of electron donation from the donor to the acceptor [31], while E(i,j) implies the strength of the donor-acceptor orbital, and strong interaction between the two orbitals is observed with higher values. As presented in Table 3 C2H2-Fe@C3N4-PEDOT demonstrated transition from LP* Fe111 to σ* C 14 -Fe111, LP* Fe111 to σ* C 13 -Fe111 and σ Fe 111 - C 113 to LP* C112 which inferred

active site for gas binding due to the strong Fe lone pair interaction with the C atoms in the system as confirmed by higher second-order perturbation energy (E2) of 201.46, 203.24, and 288.20 Kcal/mol. Furthermore, CH_4-Fe@C3N4-PEDOT demonstrated moderate interaction with 111.93, 144.87, and 146.03 Kcal/mol stabilization energy, corresponding to donor - acceptor transitions of π * C10 - N49 to π * C11 - N45, σ* C14 -Fe 111 to σ* C13 -Fe 111, and π * C13 - N21 to π * C 15 - N43 respectively. The C-H appears to be very weak compared to C_2H_2, occurring from the difference in orbital overlapping, i.e., σ bond between Fe and C and the π interactions with N. On the other hand, system H2-Fe@C_3N_4-PEDOT was suggested with moderate electron donation and acceptance due to the weaker π-bond interactions. But reflecting on the interaction strength i.e., the perturbation energy 109.80, 130.45, and 165.16 Kcal/mol. H_2-Fe@C_3N_4-PEDOT which corresponded to π * C10 - N49 to π * C11 – N45, σ* C14 -Fe 111 to σ* C13 -Fe 111, and π * C12 - N21 to π * C 9 - N48 transition shows better interaction compared to system CH_4-Fe@C_3N_4-PEDOT and less than C_2H_2-Fe@C_3N_4-PEDOT. Fe@C_3N_4-PEDOT bare surface without external adsorbates revealed the stability. The analysis revealed that C_2H_2 forms strong bonds with the center metal Fe (Chemisorption), leading to enhanced adsorption, followed by H_2 with a moderate interaction and CH_4 with a weaker interaction.

Adsorption Studies

This approach is significant to examine the adsorption potential of the adsorbent to adsorb the gases (Adsorbates) from the oil environment. The adsorption energy implies the energy difference when two molecules or atoms bind to an adsorbent. The energy change in the systems evaluates the strength of interaction between the adsorbates and the adsorbent, depending on the magnitude of the energy **[32]**. For gas sensing applications, adsorption energy values are the primary test of the applicability of a surface as a gas sensor. The adsorption energies range from 0 to −0.20 eV, (or up to −0.40 eV for larger organic molecules) is within the physisorption region, where the binding is due to van der Waals forces without any orbital overlap. Such weak interactions can easily be desorbed, but produce insufficient charge transfer to generate a measurable sensing signal. The reversible binding window (−0.20 eV to −0.40 eV) is a transition zone where marginal chemical hybridization starts to occur, in addition to the physical attraction. Surfaces with binding energies in this range are highly desirable for gas-sensing applications as the interaction energy is sufficient to cause significant changes in the electronic structure and hence the electrical response of the surface, but weak enough to release the gas molecule under mild conditions, supporting sensor regeneration without heating. Moderate chemisorption (−0.40 to −1.00 eV) implies that a real chemical bond is formed between the adsorbate and the surface, and that charge transfer is significant, often resulting in strong and reliable sensing signals. However, desorption is still thermally accessible, allowing for the possibility of recovery. When the energy is above −1.00 eV strong chemisorption is dominant, involving a significant degree of charge transfer, significant distortion in the geometry of the adsorbed molecule, or dissociative bonding. While these surfaces can exhibit dramatic responses to the target gas, they are not easily recoverable, and thus are not particularly useful for re-use as gas sensors in spite of their high sensitivity. The obtained result in Table 4 revealed that the investigated systems engage in an exothermic process, where negative adsorption energies were observed (chemisorption), i.e., favorable thermodynamics [33]. C_2H_2-Fe@C_3N_4-PEDOT (Eads = -0.871 eV) exhibits moderate chemisorption, while CH_4-Fe@C_3N_4-PEDOT and H_2-Fe@C_3N_4-PEDOT (Eads = -0.381 eV each) exhibit weak chemisorption or a reversible binding zone, consistent with the -0.4 eV stability threshold for gas sensing. All systems fall within the reusable sensor range (-0.4 to -1.0 eV). The large negative energy observed in system C_2H_2-Fe@C_3N_4-PEDOT is attributed to its molecular and bond composition, where the triple bond in acetylene (C_2H_2) interacts strongly with the Fe active site, providing a larger contact area for Van der Waals interactions, leading to improved detection. The established energy range of -0.381 to -0.871 eV indicates moderate to strong chemisorption, as required by the standard threshold **[34]**. The obtained E_{ads} is in tandem with previous studies by Gui et al. and Inah et al for the adsorption of C_2H_2, CH_4, and H_2 **[35,36]**. Hence, the moderate binding strength suggests an application requiring reversible adsorption and potential for selective gas

separation. The adsorption energy was calculated employing equation (8).

$$E_{ads} = E_{Complex} - (E_{adsorbate} + E_{surface}) \quad (8)$$

Where E_{ads} represent the investigated adsorption energy and $E_{complex}$ total energy of the gas-surface complex **(**C_2H_2-Fe@C_3N_4-PEDOT, CH_4-Fe@C_3N_4-PEDOT, and H_2-Fe@C_3N_4-PEDOT**)**, $E_{adsorbate}$ is the total energy of the isolated gas molecule (gases C_2H_2, CH_4, and H_2) before interactions. Meanwhile, $E_{Surface}$ represents total energy of the bare surface (Fe@C_3N_4-PEDOT).

Visual Studies

The reduced density gradient (RDG) of the systems was studied using the Multiwfn function and VMD software to visualize the mechanism of interaction between the chemical components of the studied systems, without an electron-sharing scenario. Non-Covalent Interactions (NCI) analysis provides insight into weak interactions, such as Van der Waals forces, dispersive forces, electrostatic forces, repulsive forces, and attractive forces of interaction between atoms or molecules [37]. These interaction forces are envisioned through inter- and intra-molecular interactions in the studied systems, depending on the electronic behaviour of each atom in the systems. With scrutiny, the QTAIM result, as discussed in the subsequent part of the study, proves a crucial alignment with NCI analysis through the values of second density Hessian eigenvalues ($\lambda 2(r)$), Laplacian value, and the electron density ($\rho(r)$). As presented in Figure 4, the systems were observed predominantly with green iso-surface, inferring weak Van der Waals interaction around the region where it is present in the systems. It also connotes the dispersive force of interactions, which can influence the stability of systems. This aligns with QTAIM when $sign\lambda 2(r)\rho(r)$ is ≈ 0, as proven by previous findings [38]. Significantly, C_2H_2-Fe@C_3N_4-PEDOT and H_2-Fe@C_3N_4-PEDOT were seen with blue iso-surfaces around metal Fe with C_2H_2 and H_2, depicting a strong attractive force of interaction resulting from hydrogen bond interaction between the adsorbates (gas C_2H_2 and H_2) and the surface, except for interaction with methane gas (CH_4) and the surface (Fe@C_3N_4-PEDOT). This can also be validated when $sign\lambda 2(r)\rho(r) < 0$ [39,40]. The systems further revealed a red iso-surface on the surface region of the studied systems, implying electrostatic force and steric repulsive interaction, which significantly influence adsorption via intermolecular interaction within the systems. The interaction can be confirmed with QTAIM when $sign\lambda 2(r)\rho(r) > 0$ [41].

Unequivocally, the types of interaction that exist between the adsorbates (gas C2H2, CH4, H2) and the surface (Fe@C3N4-PEDOT) are evident that it may influence the adsorption and sensing potential of the studied surface against the gases.

CONCLUSION

This study was done to investigate the adsorption or gas-sensing ability of Fe@C_3N_4-PEDOT nanomaterial on interaction with three gases: C_2H_2, CH_4, and H_2 using the density functional theory (DFT) method. The nanomaterial showed good electronic properties upon Fe-doping, predominantly in the detection of acetylene. The adsorption energy values established spontaneous and stable interactions, with C_2H_2 showing the most favourable interaction (-0.871 eV). Conversely, the materials showed high conductivity and sensing efficiency as seen through the HOMO-LUMO and DOS analysis, indicating a decrease in energy gap and improved charge mobility. Furthermore, the quantum descriptors like reactivity, softness, and electrophilicity support the sensing ability of the nanomaterial. A strong orbital interaction and chemisorption, mostly with acetylene, show that the Fe@C_3N_4-PEDOT material is highly responsive and selective, as seen in the NBO analysis. The adsorption energies for CH_4 and H_2 (-0.381 eV), consistent with weak chemisorption, suggest reversible adsorption behaviour favourable for reusable gas sensor applications, while C_2H_2 (-0.871 eV) remains within the reusable sensor range. These results show the excellent performance of Fe@C3N4-PEDOT, making it highly potent as a gas-sensing material due to its sensitivity, stability, and efficiency, especially with high selectivity towards acetylene gas. The present investigation is based on gas-phase DFT calculations and considers only Fe as the dopant species in the g-C_3N_4/PEDOT hybrid system. Therefore, the effects of the transformer oil matrix, solvent interactions, temperature fluctuations, and competing gas adsorption were not explicitly included in the simulations. Future studies should incorporate more realistic oil-environment models, explore alternative

dopant metals and dopant concentrations, and validate theoretical predictions through experimental sensor fabrication and performance testing under practical transformer operating conditions.

Declarations

Competing Interest

The authors declare that they have no known competing financial interests or personal relationships that could have appeared to influence the work reported in this paper.

Ethical Approval

Not applicable. This study did not involve human research participants or live vertebrates.

Consent to Participation

Not applicable. This study did not involve human research participants.

Consent to Publish

Not applicable. No participants were involved in this study.

Funding

This research was not funded by any Governmental or Non-governmental agency.

Availability of data and material

All data are contained within the manuscript and the manuscript supporting information (SI) documents. Optimized (log) files are available on request.

Authors' Contribution

1. Investigation, Methodology, Writing – original draft, Project administration.
2. Writing – original draft, Data curation, Formal analysis, Investigation;
3. Conceptualization, Supervision, Visualization, Writing – review & editing.
4. Methodology, Writing – original draft, Writing – review & editing, Validation

REFERENCES

Ma, G. M., Zhao, S. J., Jiang, J., Song, H. T., Li, C. R., Luo, Y. T., & Wu, H. (2017). Tracing acetylene dissolved in transformer oil by tunable diode laser absorption spectrum. *Scientific reports*, *7*(1), 14961.

Aciu, A. M., Nicola, C. I., Nicola, M., & Nițu, M. C. (2021). Complementary analysis for DGA based on Duval methods and furan compounds using artificial neural networks. *Energies*, *14*(3), 588.

Soni, R., Joshi, S., Lakhiani, V., & Jhala, A. (2015). Condition monitoring of power transformer using dissolved gas analysis of mineral oil: a review. *Int. J. Adv. Eng. Res. Dev*, *3*, 2348-4470.

Atrafi, M. A., & Marufov, I. M. (2023). Effect of partial discharge on physical and chemical properties of transformer oil. *International Journal of Thermal and Power Engineering*, *15*(2), 101-105.

Hussain, M. R., Refaat, S. S., & Abu-Rub, H. (2021). Overview and partial discharge analysis of power transformers: A literature review. *Ieee Access*, *9*, 64587-64605.

Mahdi, A. S., Abdul-Malek, Z., & Arshad, R. N. (2022). SF 6 decomposed component analysis for partial discharge diagnosis in GIS: A review. *Ieee Access*, *10*, 27270-27288.

Ezennubia, V., & Vilcáez, J. (2023). Removal of oil hydrocarbons from petroleum produced water by indigenous oil degrading microbial communities. *Journal of Water Process Engineering*, *51*, 103400.

Yemashova, N. A., Murygina, V. P., Zhukov, D. V., Zakharyantz, A. A., Gladchenko, M. A., Appanna, V., & Kalyuzhnyi, S. V. (2007). Biodeterioration of crude oil and oil derived products: a review. *Reviews in Environmental Science and Bio/Technology*, *6*, 315-337.

Fan, J., Liu, Z., Meng, A., Yin, H., Sun, Q., Bin, F., & Jiang, Q. (2019). Characteristics of tin oxide chromatographic detector for dissolved gases analysis of transformer oil. *IEEE Access*, *7*, 94012-94020.

Cheng, L., & Yu, T. (2018). Dissolved gas analysis principle-based intelligent approaches to fault diagnosis and decision making for large oil-immersed power transformers: A survey. *Energies*, *11*(4), 913.

Baig, N., Kammakakam, I., & Falath, W. (2021). Nanomaterials: A review of synthesis methods, properties, recent progress, and challenges. *Materials advances*, *2*(6), 1821-1871.

Jin, W., & Maduraiveeran, G. (2019). Recent advances of porous transition metal-based nanomaterials for electrochemical energy conversion and storage applications. *Materials Today Energy*, *13*, 64-84.

Jose, A., Mathew, T., Fernández-Navas, N., & Querebillo, C. J. (2024, April). Porous inorganic nanomaterials: Their evolution towards hierarchical porous nanostructures. In *Micro* (Vol. 4, No. 2, pp. 229-280). MDPI.

He, X., Gui, Y., Xie, J., Liu, X., Wang, Q., & Tang, C. (2020). A DFT study of dissolved gas (C2H2, H2, CH4) detection in oil on CuO-modified BNNT. *Applied Surface Science*, *500*, 144030.

Zhou, Q., Zhang, G., Tian, S., & Zhang, X. (2020). First-principles insight into Pd-doped ZnO monolayers as a promising scavenger for dissolved gas analysis in transformer oil. *ACS omega*, *5*(28), 17801-17807.

Xu, Z. (2023). Ni-decorated PtS2 monolayer as a strain-modulated and outstanding sensor upon dissolved gases in transformer oil: a first-principles study. *ACS omega*, *8*(6), 6090-6098.

Elemike, E. E., Onunkwo, I. C., Ididama, O. E., Okorodudu, O. E., Okogbenin, I. P., Egbele, O. R., ... & Aziza, A. E. (2024). Exploring the production and storage of hydrogen energy using graphitic carbon nitride (g-C3N4). *International Journal of Hydrogen Energy*, *70*, 212-232.

Heydari Gharahcheshmeh, M., Dautel, B., & Chowdhury, K. (2025). Enhanced carrier mobility and thermoelectric performance by nanostructure engineering of PEDOT thin films fabricated via the OCVD method using SbCl5 oxidant. *Advanced Functional Materials*, *35*(10), 2418331.

Roy, L. E., Hay, P. J., & Martin, R. L. (2008). Revised basis sets for the LANL effective core potentials. *Journal of chemical theory and computation*, *4*(7), 1029-1031.

Bauschlicher Jr, C. W. (1995). A comparison of the accuracy of different functionals. *Chemical Physics Letters*, *246*(1-2), 40-44.

Humphrey, W., Dalke, A., & Schulten, K. (1996). VMD: visual molecular dynamics. *Journal of molecular graphics*, *14*(1), 33-38.

Jiang, W., Zeng, Q., Zhang, Y., Wang, G., Sun, K., Xu, M., Chen, D., & Jia, P. (2025). Adsorption and sensing characteristics of transition metal (Au, Fe, Pt, Rh and Cu) doped WS_2 on dissolved gases in transformer oil: A DFT perspective. *Computational and Theoretical Chemistry*, 2210-271X. https://doi.org/10.1016/j.comptc.2025.xxxxxx.

Fan, Y., Zhang, J., Qiu, Y., Zhu, J., Zhang, Y., & Hu, G. (2017). A DFT study of transition metal (Fe, Co, Ni, Cu, Ag, Au, Rh, Pd, Pt and Ir)-embedded monolayer MoS_2 for gas adsorption. *Computational Materials Science*, 138, 255–266. https://doi.org/10.1016/j.commatsci.2017.06.033

Di Valentin, C., & Pacchioni, G. (2014). Spectroscopic properties of doped and defective semiconducting oxides from hybrid density functional calculations. *Accounts of chemical research*, *47*(11), 3233-3241.

Sahoo, S., Reber, A. C., & Khanna, S. N. (2016). Effect of location and filling of d-states on methane activation in single site Fe-based catalysts. *Chemical Physics Letters*, *660*, 48-54.

Braga, L. S., Leal, D. H., Kuca, K., & Ramalho, T. C. (2020). Perspectives on the role of the frontier effective-for-reaction molecular orbital (FERMO) in the study of chemical reactivity: an updated review. *Current Organic Chemistry*, *24*(3), 314-331.

Francis, M., & Roy, S. (2023). Stabilisation and reactivity studies of donor-base ligand-supported gallium-phosphides with stronger binding energy: a theoretical approach. *RSC advances*, *13*(12), 7738-7751.

Anadebe, V. C., Lgaz, H., Aldalbahi, A., Lee, H. S., Mathias, G. E., Badeji, A. A., ... & Ebenso, E. E. (2025). Interfacial inhibition of mild steel corrosion by Abemaciclib and Abrocitinib in acidic media: Insights from density functional theory and molecular dynamics simulations. *ChemistrySelect*, *10*(32), e03502.

Zhou, B., Hu, Z., Jiang, Y., He, X., Sun, Z., & Sun, H. (2018). Benchmark study of ionization potentials and electron affinities of armchair single-walled carbon nanotubes using density functional theory. *Journal of Physics: Condensed Matter*, *30*(21), 215501.

von Szentpály, L. (2015). Physical basis and limitations of equalization rules and principles: valence-state electronegativity and valence-pair-affinity versus operational chemical potential. *Quantum Matter*, *4*(1), 47-55.

Weinhold, F., Landis, C. R., & Glendening, E. D. (2016). What is NBO analysis and how is it useful? *International reviews in physical chemistry*, *35*(3), 399-440.

Miah, M. H., Hossain, M. R., Islam, M. S., Ferdous, T., & Ahmed, F. (2021). A theoretical study of allopurinol drug sensing by carbon and boron nitride nanostructures: DFT, QTAIM, RDG, NBO and PCM insights. *RSC advances*, *11*(61), 38457-38472.

Eberle, B., Hübner, O., Ziesak, A., Kaifer, E., & Himmel, H. J. (2015). What makes a strong organic electron donor (or acceptor)?. *Chemistry–A European Journal*, *21*(23), 8578-8590.

Shabir, F., Sultan, M., Miyazaki, T., Saha, B. B., Askalany, A., Ali, I., ... & Shamshiri, R. R. (2020). Recent updates on the adsorption capacities of adsorbent-adsorbate pairs for heat transformation applications. *Renewable and Sustainable Energy Reviews*, *119*, 109630.

Saha, P., & Chowdhury, S. (2011). Insight into adsorption thermodynamics. *Thermodynamics*, *16*, 349-364.

Gas sensing Mbonu, I. J., Eze, G. E., Badeji, A. A., & Eno, E. A. (2026). Surface Tailoring of Porphyrin Via Nickel-Encapsulation and Germanium-Doping Towards the Detection of Decomposed Transformer Oil Pollutants (C2H2, C2H4, H2 and CO): A Computational Study. *Chemistry Africa*, *9*(4), 176.

Králik, M. (2014). Adsorption, chemisorption, and catalysis. *Chemical Papers*, *68*(12), 1625-1638.

Gui, Y., Hu, X., Zhu, S., & Chen, X. (2022). A DFT study of transition metal (Ag, Au, Co) modified SnS2 monolayer for the detection and adsorption of the representative gases (NH3, Cl2, and C2H2) in greenhouses. *Materials Today Communications*, *33*, 104618.

Inah, B. E., Eze, J. F., Louis, H., Edet, H. O., Gber, T. E., Eno, E. A., ... & Adeyinka, A. S. (2023). Adsorption and gas-sensing investigation of oil dissolved gases onto nitrogen and sulfur doped graphene quantum dots. *Chemical Physics Impact*, *7*, 100265.

Sarala, S., Geetha, S. K., Muthu, S., & Irfan, A. (2021). Computational investigation, comparative approaches, molecular structural, vibrational spectral, non-covalent interaction (NCI), and electron excitations analysis of benzodiazepine derivatives. *Journal of Molecular Modeling*, *27*(9), 266.

Alonso, M., Woller, T., Martín-Martínez, F. J., Contreras-García, J., Geerlings, P., & De Proft, F. (2014). Understanding the Fundamental Role of π/π, σ/σ, and σ/π Dispersion Interactions in Shaping Carbon-Based Materials. *Chemistry–A European Journal*, *20*(17), 4931-4941.

de Oliveira Neto, J. G., Souza Junior, M. V., Ayala, A. P., Nogueira, C. E., Souto, E. B., dos Santos, A. O., & de Sousa, F. F. (2024). Structural Design, H-Bonding Interactions, Vibrational Properties, Periodic-DFT Calculations, and Antibacterial Activity of a Nicotinamide Cocrystal Using Tetradecanoic Acid as a Coformer. *Crystal Growth & Design*, *24*(22), 9810-9823.

Chakraborty, J. (2022). An account of noncovalent interactions in homoleptic palladium (II) and platinum (II) complexes within the DFT framework: A correlation between geometries, energy components of symmetry-adapted perturbation theory and NCI descriptors. *Heliyon*, *8*(11).

Wazzan, S., & Ozalan, N. U. (2023). Graph Energy Variants and Topological Indices in Platinum Anticancer Drug Design: Mathematical Insights and Computational Analysis with DFT and QTAIM. *Journal of Mathematics*, *2023*(1), 5931820.

Rojas-Valencia, N., Gómez, S., Guerra, D., & Restrepo, A. (2020). A detailed look at the bonding interactions in the microsolvation of monoatomic cations. *Physical Chemistry Chemical Physics*, *22*(23), 13049-13061.

Badeji, A. A., Pathmanathan, K., Abdullah, H. Y., Hossain, I., & Runde, M. (2025). Unveiling the catalytic versatility of transition metal-doped coal char systems for hydrogen evolution reaction: a first-principles approach. *Chemical Physics*, 112882.

Zhou, F., Liu, R., Li, P., & Zhang, H. (2015). On the properties of S⋯ O and S⋯ π noncovalent interactions: the analysis of geometry, interaction energy and electron density. *New Journal of Chemistry*, *39*(3), 1611-1618.

Savin, A., Nesper, R., Wengert, S., & Fässler, T. F. (1997). ELF: The electron localization function. *Angewandte Chemie International Edition in English*, *36*(17), 1808-1832.

Silva Lopez, C., & R de Lera, A. (2011). Bond ellipticity as a measure of electron delocalization in structure and reactivity. *Current Organic Chemistry*, *15*(20), 3576-3593.